Research Article | Vol. 11, No. 2 / 1 February 2020 / Biomedical Optics Express 963
Biomedical Optics EXPRESS

Diagnosis of methylglyoxal in blood by using far-infrared spectroscopy and o-phenylenediamine derivation

XU WU,[1] YANG DAI,[2] LIPING WANG,[1] YAN PENG,[1,3,4] LIN LU,[2,5] YIMING ZHU,[1,3,6] YIJUE SHI,[2] AND SONGLIN ZHUANG[1]

[1]*Terahertz Technology Innovation Research Institute, Shanghai Key Lab of Modern Optical System, Terahertz Science Cooperative Innovation Center, University of Shanghai for Science and Technology, Shanghai, China*
[2]*Department of Cardiology, Rui Jin Hospital, Shanghai Jiaotong University School of Medicine, Shanghai 200025, China*
[3]*Shanghai Institute of Intelligent Science and Technology, Tongji University, Shanghai, China*
[4]*py@usst.edu.cn*
[5]*rjlulin1965@163.com*
[6]*ymzhu@usst.edu.cn*

Abstract: Methyglyoxal (MGO) is an important pathological factor for diabetic cardiovascular complications. Conventional methods for MGO detection in biological samples, such as high performance liquid chromatography (HPLC)-UV spectrometry, LC-fluorescence spectrometry, and HPLC-mass spectrometry, are time-consuming, high-cost, and complicated. Here, we present a method for MGO quantitative detection based on far-IR spectral analyses. Our method uses o-phenylenediamine (OPD) to produce a chemical reaction with MGO, which results in multiple fingerprint feature changes associated with the molar ratio of MGO and OPD. We use the linear relationship between MGO concentration and peak intensity of the reaction product to quantitatively determine MGO concentration. The corresponding linear detectable range is 5~2500 nmol/mL nmol per mL with a correlation coefficient of 0.999. This quantitative method is also tested by blood samples with adjusted MGO concentrations, and shows 95% accuracy with only 30s testing time. Our method provides a fast, simple and economical approach to determining MGO concentration in blood.

1. Introduction

Diabetes mellitus is estimated to affect more than 415 million adults worldwide. The prevalence is increasing, and it is expected that more than 640 million adults will have diabetes by 2040 [1]. Patients with diabetes are at high risk for adverse outcomes from atherosclerotic cardiovascular disease [2,3], heart failure [4], and renal disease [5]. As a result of this intersection of diabetes, atherosclerotic cardiovascular disease, and heart failure, the importance of determining diabetes therapies that are not only safe but also effective in reducing cardiovascular risk is paramount. At present, the main diagnostic methods for diabetic cardiovascular complications are coronary angiography, magnetic resonance (MR) imaging, and computed tomographic (CT) angiography. Coronary angiography is the golden standard for diagnosing diabetic cardiovascular complications, but it is invasive and its intravascular 2D imaging cannot provide enough information for accurate surgical design [6]. While for MR imaging and CT angiography, gadolinium-based contrast agents are unavoidable and the cost is high [7,8].

As an important pathogenic factor of diabetic cardiovascular complications, methylglyoxal (MGO) has attracted more and more attention since 2012 [9–13]. In 2017, Y. Dai et al. found that the accumulation of MGO plays an important role in the formation of glycated apolipoprotein, which can lead to atherogenesis and eventual cardiovascular complications [14]. In 2018, A.

#381542 https://doi.org/10.1364/BOE.381542
Journal © 2020 Received 28 Oct 2019; revised 7 Jan 2020; accepted 8 Jan 2020; published 17 Jan 2020

Biomedical Optics EXPRESS

Moraru et al. demonstrated that MGO concentration in blood is critical for the progression and initiation of diabetic cardiovascular complications [15]. At present, the research methods for MGO analysis are high performance liquid chromatography (HPLC)-UV spectrometry [16–18], LC-fluorescence spectrometry [19,20], and HPLC-mass spectrometry [21,22]. These methods mainly depend on MGO separation by chromatography technique. However, their disadvantages, including expensive instruments, complicated operation flow, and long processing-time, determine these methods are not suitable for routine clinical use [23,24]. There is no clinical method for MGO identification in blood now.

In this paper, we present a fast and economical detection method for MGO identification in blood. Considering that the characteristic absorption peaks of MGO are not sharp or intense enough to be accurately identified at low concentration, we used o-phenylenediamine (OPD) to convert MGO into a new chemical product, which has sharp and strong absorption peaks in the far-IR range. Depending on the far-IR spectral changes before and after the reaction of MGO with OPD, MGO concentration can be quantitatively detected from 5 to 2500 nmol/mL, with an accuracy of 95%.

2. Experimental setup and materials

The experimental setup is a commercial Fourier transform infrared spectrometer (Vectex 80v, Bruker Optics). The far-infrared (IR) light emits from a water-cooled mercury and is detected by a DLaTGS/polyethylene detector. Thus the spectral region effectively covers 30~680 cm^{-1}, and the signal to noise ratio (SNR) is better than 10000:1. All the spectra are measured with a resolution of 2 cm^{-1}, a scan number of 64, and a scan speed of 5 kHz in the spectral range from 30 cm^{-1} to 500 cm^{-1}.

MGO aqueous solution (CAS: 78-98-8, 6.5 mol/L), OPD powders (CAS: 95-54-5, 99.5% purity), and liquid 2-methylquinoxaline (CAS: 7251-61-8, 97% purity) were purchased from Sigma-Aldrich. All chemicals were used as received without further purification. Ultra-pure water was provided by a lab water purification system (ELGA, UK). Human blood samples were obtained from healthy volunteers, provided by the Department of Cardiology, Rui Jin Hospital, Shanghai Jiaotong University School of Medicine (Shanghai, China). Blood samples were firstly treated with acetonitrile to eliminate the interference of albumin and immunoglobulins (protein-free serum) [25], then mixed with MGO solution through standard addition method [26], leading to MGO blood mixtures with MGO concentrations of 100, 150 and 250 nmol/mL, respectively. These mixtures were used to test the reliability of the detection method presented here. Silicon wafer (0.3 mm thickness) was used as the reference substance for liquid sample measurement. Its corresponding spectrum was collected as the reference spectrum.

3. Results and discussion

3.1. Fingerprint spectra of MGO, OPD and their reaction product

Firstly, the fingerprint spectrum of pure MGO was measured in the range from 30 to 500 cm^{-1} [Fig. 1(a)]. MGO sample was prepared by dropping 6 μL of MGO solution (~39 μmol) onto a Si wafer and drying under a high-purity N_2 flow, leading to a spot of 10 mm in diameter. As shown in Fig. 1(a), the MGO spectrum can be divided mainly into three broad absorption bands. The largest band is centered at 86.7 cm^{-1}. The other two bands have small peaks at 254.3 cm^{-1}, 280.9 cm^{-1}, 376.2 cm^{-1}, and 405.3 cm^{-1}. However, the 86.7 cm^{-1} band is too broad, and the other peaks are too weak, which cannot be used for the effective identification of MGO, especially at low concentration.

To solve this problem, we use OPD to react with MGO, leading to multiple changes of fingerprint features according to the molar ratio change between MGO and OPD. The corresponding chemical reaction equation is described in Fig. 1(b). One molecule of MGO combines with one molecule

Biomedical Optics EXPRESS

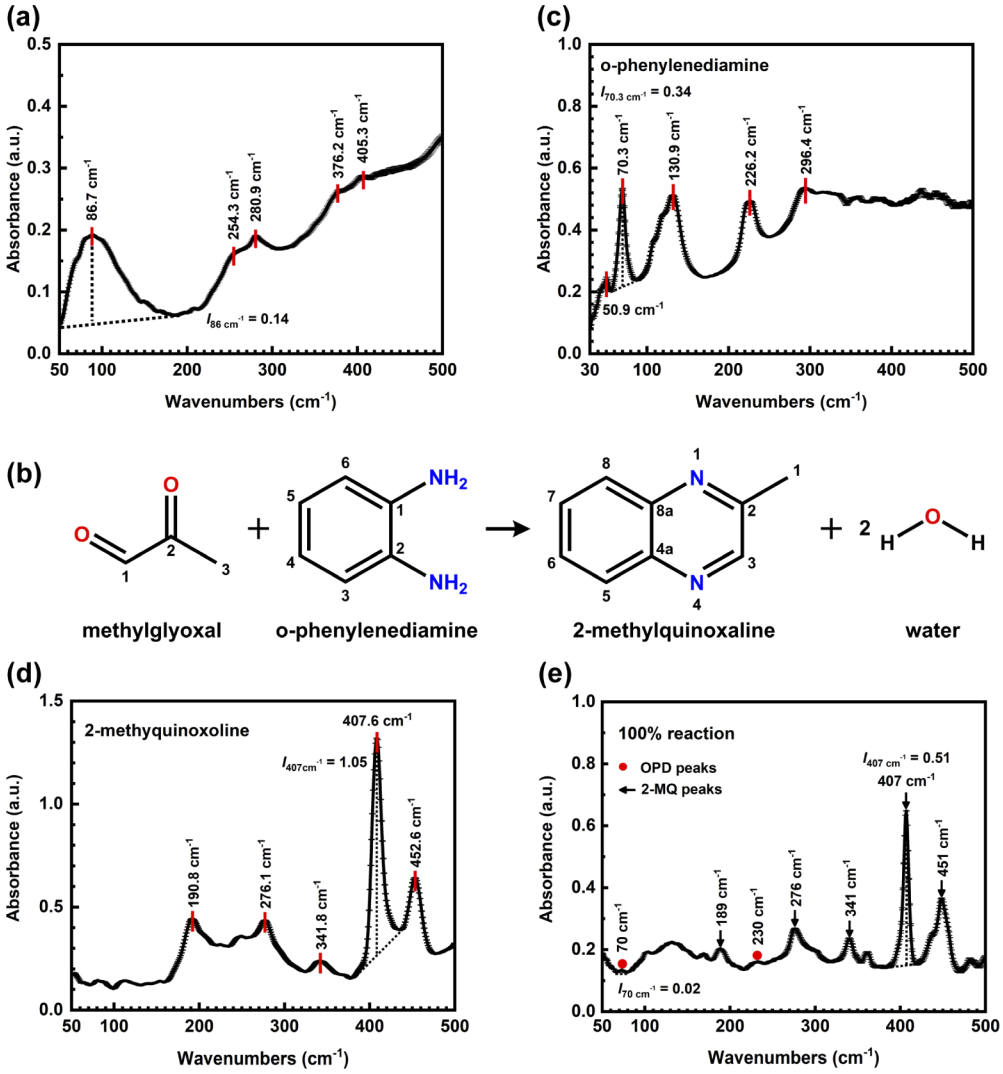

Fig. 1. Fingerprint spectrum of (a) MGO, (c) OPD, (d) 2-methyquinoxoline (2-MQ) and (e) the reaction product from the same molar amount of MGO and OPD. (b) Chemical reaction equation of MGO and OPD.

of OPD to form one molecule of 2-MQ and one molecule of water. In the experiments, OPD sample was prepared by compressing 2 mg of OPD powders (~18.5 μmol) into a smooth pellet with a diameter of 13 mm. 2-MQ sample was prepared by directly spotting 5 μL of liquid 2-methylquinoxaline (~39 μmol) onto a Si wafer. Then these samples were measured by a far-IR spectrometer. As shown in Fig. 1(c), OPD exhibits a small absorption peak at 50.9 cm^{-1}, and three sharp peaks at 70.3 cm^{-1}, 130.9 cm^{-1}, and 226.2 cm^{-1}, respectively. As shown in Fig. 1(d), 2-MQ has a strong and sharp absorption peak centered at 407.6 cm^{-1}, along with four relatively weak peaks at 190.8 cm^{-1}, 276.1 cm^{-1}, 341.8 cm^{-1}, and 452.6 cm^{-1}, respectively. We notice that the characteristic peaks of MGO, OPD, and 2-MQ are separated from each other greatly, benefiting for the spectral identification and analysis. Furthermore, for the highest 2-MQ peak at 407.6 cm^{-1} ($I_{407cm^{-1}}$=1.05), its intensity is 7.5 times as that of the highest MGO absorption peak at 86.7 cm^{-1} ($I_{86cm^{-1}}$=0.14), although the molar quantity of the 2-MQ sample and the MGO

Biomedical Optics EXPRESS

sample is almost the same (~39 μmol). Therefore, at the same low MGO concentration, the 2-MQ peaks are more easily identified than that of the MGO peaks.

Then, we performed a chemical reaction starting with equal parts of MGO and OPD, to make sure the efficiency of the reaction and the purity of the reaction product. The experimental formulation is presented in Table 1 [equivalent MGO reaction (MGO = OPD)]. The detailed reaction process is described as follows: 1) MGO aqueous solution (1 mol/L, 20 μL) and OPD aqueous solution (1 mol/L, 20 μL) are mixed and stabilized for eight hours. 2) The reaction solution is dotted on Si wafer and left to dry. 3) The dried sample is measured by a far-IR spectrometer. The spectrum, as shown in Fig. 1(e), has two small OPD peaks at 70 cm^{-1} and 230 cm^{-1}, as well as five characteristic peaks of 2-MQ, which are respectively located at 189 cm^{-1}, 276 cm^{-1}, 341 cm^{-1}, 407 cm^{-1}, and 451 cm^{-1}. Among these peaks, the 407 cm^{-1} peak with the highest intensity is selected to monitor the yield of 2-MQ. In comparison with the 407 cm^{-1} peak in Fig. 1(d) ($I_{407\ cm^{-1}}$=1.05, 39 μmol 2-MQ), the intensity of the 407 cm^{-1} peak in Fig. 1(e) is 0.51, indicating that the corresponding yield of 2-MQ is ~18.9 μmol. Similarly, in comparison with the 70 cm^{-1} peak in Fig. 1(c) ($I_{70cm^{-1}}$=0.34, 18.5 μmol OPD), the residue amount of OPD is calculated to be ~1.1 μmol according to the intensity of the 70 cm^{-1} peak in Fig. 1(e) ($I_{70cm^{-1}}$=0.02). The MGO concentration can be deduced by combining the yield of 2-MQ and the residue amount of OPD [Fig. 1(b)]. Basing on the values above, the reaction efficiency is calculated to be 90%. Also, the chemical reaction of MGO and OPD has the advantages of a simple technological process and ambient temperature in nearly neutral aqueous media.

Table 1. Representative examples of equivalent MGO, excess MGO, and insufficient MGO reactions

MGO (μmol)	OPD (μmol)	MGO:OPD (OPD percentage)	Reaction name	Reaction type
20	20	4:4 (100%)	100% reaction	equivalent MGO reaction (MGO = OPD)
20	5	4:1 (25%)	25% reaction	excess MGO reaction (MGO > OPD)
20	10	4:2 (50%)	50% reaction	
20	30	4:6 (150%)	150% reaction	insufficient MGO reaction (MGO < OPD)
20	40	4:8 (200%)	200% reaction	

3.2. Qualitative and quantitative analysis of MGO

Considering that MGO concentration in human blood varies from person to person, it is important to choose an appropriate amount of OPD to react and then determine the unknown concentration of MGO. Here, we did four experiments to explore how the spectrum of the reaction product changes with the molar ratio of MGO:OPD. Detailed experimental formulations are shown in Table 1. In these reactions, MGO is kept at 20 μmol and OPD is varied from 5 to 40 μmol. For simplicity, these reactions are named after the initial molar percentage of OPD.

The spectra of the chemical products starting with different molar ratios of MGO and OPD are shown in Fig. 2(a-b). 1) 100% reaction represents the equivalent MGO reaction [MGO = OPD, see Fig. 1(e)]. 2) 25% and 50% reaction represent the excess MGO reactions [MGO > OPD, see Fig. 2(a)]. In comparison with the product from the equivalent MGO reaction, the products from excess MGO reactions only have four 2-MQ peaks, which are respectively located at 189 cm^{-1}, 296 cm^{-1}, 407 cm^{-1}, and 452 cm^{-1} [Fig. 2(a)]. The intensities of the 2-MQ peaks from the 50% reaction are higher than those of the corresponding peaks from the 25% reaction, suggesting that the 50% reaction yields more 2-MQ than the 25% reaction. 3) 150% and 200% reactions stand for the insufficient MGO reaction [MGO < OPD, see Fig. 2(b)]. For products from insufficient MGO reactions, there are not only these 2-MQ peaks but also four OPD peaks, which are respectively located at 70 cm^{-1}, 130 cm^{-1}, 226 cm^{-1} and 296 cm^{-1} [Fig. 2(b)]. Compared to the product

Biomedical Optics EXPRESS

from the 150% reaction, the product from 200% reaction has higher OPD peaks, indicating more residual unreacted OPD in the 200% reaction.

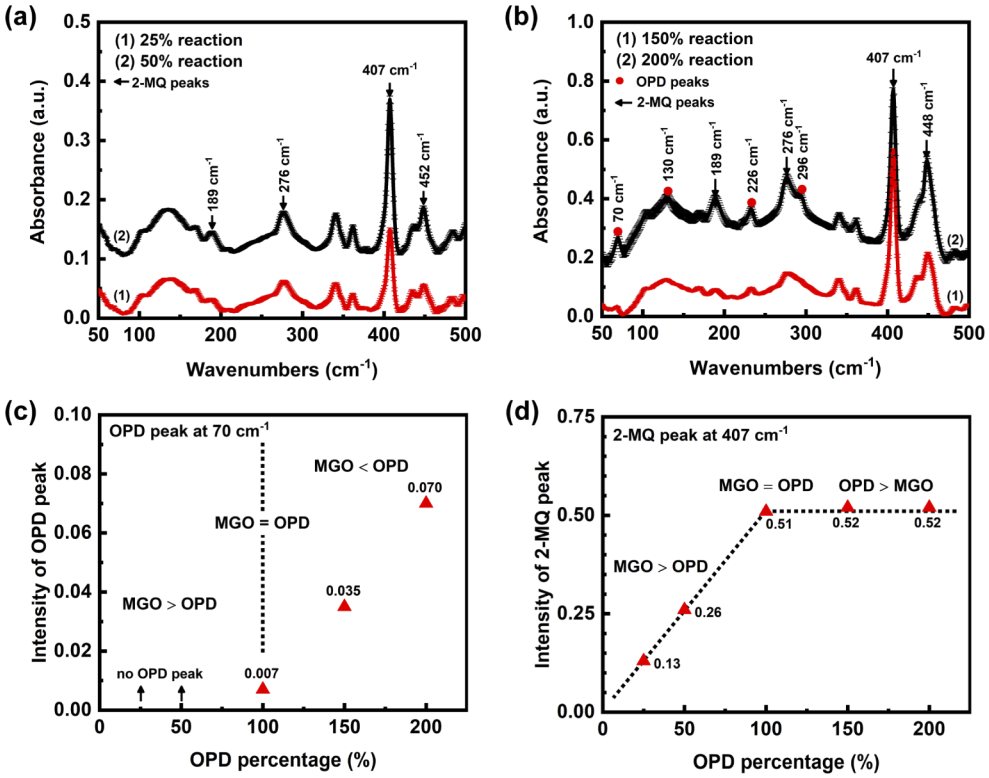

Fig. 2. Spectra of products from reactions with different molar ratios of MGO and OPD: (a) excess MGO reaction and (b) insufficient MGO reaction. Intensities of (c) OPD peak at 70 cm^{-1} and (d) 2-MQ peak at 407 cm^{-1} as a function of the OPD percentage.

To show the peak intensity changes more clearly, OPD peak at 70 cm^{-1} and 2-MQ peak at 407 cm^{-1} are selected as two typical features, as shown in Fig. 2(c-d). With an increasing relative percentage of OPD in the reagents, the intensity change of the OPD peak follows the order from invisible, negligible (OPD percentage < 100%), to gradually strengthened (OPD percentage > 100%). While for the 2-MQ peak [Fig. 2(d)], its intensity increases almost linearly until the OPD percentage grows up to 100%. Further increase of OPD percentage cannot result in any noticeable intensity change at 407 cm^{-1}.

Basing on the linear relation between the intensity of the 407 cm^{-1} peak and the concentration of MGO, a calibration curve of MGO is built up. As illustrated in Fig. 3, the linear regression equation is

$$C_{MGO} = 33.82 \times I_{407cm^{-1}} \times 10^3 \quad (1)$$

$I_{407cm^{-1}}$ represents the measured intensity of 407 cm^{-1} peak (a.u.), and C_{MGO} represents the concentration of MGO (nmol/mL), in a range of 5~2500 nmol/mL. The corresponding correlation coefficient (R^2) is 0.999. This fact indicates that the intensity at 407 cm^{-1} has a highly linear response to the MGO concentration over four orders of magnitude.

The limit of detection (LoD) of this method is determined by Eq. (2). [27]

$$LoD = 3 \times S.D./slope \quad (2)$$

Biomedical Optics EXPRESS

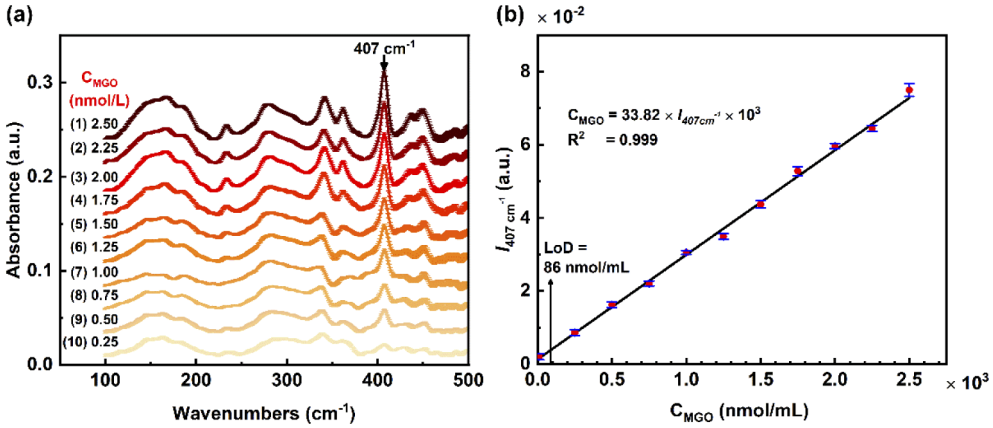

Fig. 3. (a) Spectral changes of the reaction products and (b) corresponding intensity changes of the 2-MQ peak at 407 cm^{-1} due to the increasing MGO concentrations.

S.D. is the standard deviation, 8.43274×10^{-4}, corresponding to the lowest detectable concentration. *slope* is $1/(33.82\times10^{3})$, representing the slope of the intensity of 407 cm^{-1} peak. Here LoD is 86 nmol/mL.

3.3. Quantitative detection of MGO in blood

After confirmed the limit of detection and the linear coverage range of this detection method, we then verify its reliability and effectiveness by testing blood samples. These samples are prepared by adjusting MGO concentration in protein-free serum. Each sample was tested ten times, and each test took about 30s.

The results are shown in Fig. 4. For blood samples, the intensity of 407 cm^{-1} peak increases linearly with MGO concentration. At 407 cm^{-1}, the measured peak intensity is 0.0036 ± 0.0012 for 100 nmol/mL MGO, 0.0053 ± 0.0013 for 150 nmol/mL MGO, and 0.0073 ± 0.0005 for 250 nmol/mL MGO, respectively. According to the Eq.(1), the predictive intensity at 407 cm^{-1} is

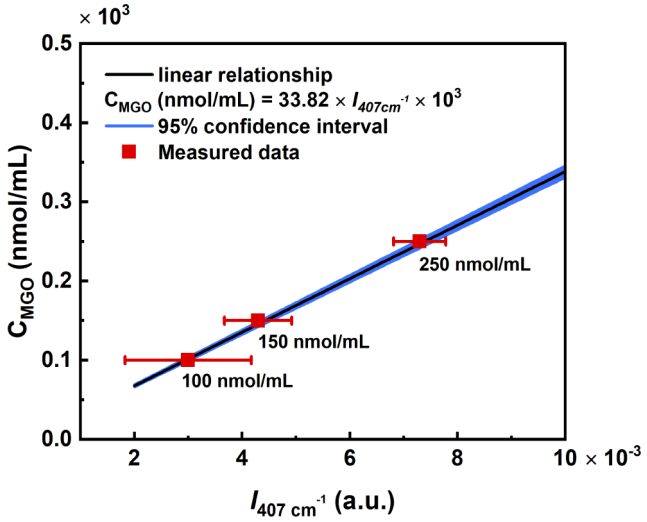

Fig. 4. Test results of MGO concentration in protein-free serum.

Biomedical Optics EXPRESS

0.0030 for 100 nmol/mL MGO, 0.0045 for 150 nmol/mL MGO, and 0.0060 for 250 nmol/mL MGO, respectively. These experimental results lie within the range defined by the 95% confidence interval, fitting well with the theoretical prediction. This result indicates that this method has good reliability in the quantitative detection of MGO in blood.

4. Conclusion

We demonstrate a method for determining the concentration of methylglyoxal (MGO) in blood. The chemical reaction between MGO and o-phenylenediamine (OPD) is used to induce multiple fingerprint feature changes according to the molar ratio change between MGO and OPD. By adjusting the relative molar ratio of MGO and OPD, we find that the absence of the OPD peaks, especially at 70 cm^{-1} and 230 cm^{-1}, can be served as signatures for abnormally high MGO concentration. Besides, the 407 cm^{-1} peak has a linear response to the blood MGO concentration, over four orders of magnitude (5~2500 nmol/mL) with a good correlation (R^2=0.999). This method is used to test protein-free serum samples with different MGO concentrations and shows good reliability (95% accuracy). The detection method is easy to operate and economical. This work has a great meaning for the future clinical detection of MGO in many diseases.

Funding

National Major Project of Scientific Instrument and Equipment Development (2017YFF0106300); National Natural Science Foundation of China (61805140, 61922059, 61771314, 61722111); Shanghai Rising-Star Program (17QA1402500).

Disclosures

The authors have declared no conflicts of interest.

References

1. K. Ogurtsova, J. D. da Rocha Fernandes, Y. Huang, U. Linnenkamp, L. Guariguata, N. H. Cho, D. Cavan, J. E. Shaw, and L. E. Makaroff, "IDF Diabetes Atlas: Global estimates for the prevalence of diabetes for 2015 and 2040," Diabetes Res. Clin. Pract. **128**, 40–50 (2017).
2. S. M. Donahoe, G. C. Stewart, C. H. McCabe, S. Mohanavelu, S. A. Murphy, C. P. Cannon, and E. M. Antman, "Diabetes and Mortality Following Acute Coronary Syndromes," JAMA **298**(7), 765–775 (2007).
3. V. L. Roger, A. S. Go, D. M. Lloyd-Jones, R. J. Adams, J. D. Berry, T. M. Brown, M. R. Carnethon, S. Dai, G. de Simone, E. S. Ford, C. S. Fox, H. J. Fullerton, C. Gillespie, K. J. Greenlund, S. M. Hailpern, J. A. Heit, P. M. Ho, V. J. Howard, B. M. Kissela, S. J. Kittner, D. T. Lackland, J. H. Lichtman, L. D. Lisabeth, D. M. Makuc, G. M. Marcus, A. Marelli, D. B. Matchar, M. M. McDermott, J. B. Meigs, C. S. Moy, D. Mozaffarian, M. E. Mussolino, G. Nichol, N. P. Paynter, W. D. Rosamond, P. D. Sorlie, R. S. Stafford, T. N. Turan, M. B. Turner, N. D. Wong, and J. Wylie-Rosett, "Heart disease and stroke statistics-2011 update: a report from the American Heart Association," Circulation **123**(4), e18–e209 (2011).
4. F. S. Ahmad, H. Ning, J. D. Rich, C. W. Yancy, D. M. Lloyd-Jones, and J. T. Wilkins, "Hypertension, Obesity, Diabetes, and Heart Failure-Free Survival," JACC: Heart Failure **4**(12), 911–919 (2016).
5. E. Ritz and S. R. Orth, "Nephropathy in Patients with Type 2 Diabetes Mellitus," N. Engl. J. Med. **341**(15), 1127–1133 (1999).
6. G. S. Mintz and G. Guagliumi, "Intravascular imaging in coronary artery disease," Lancet **390**(10096), 793–809 (2017).
7. P. S. Douglas, U. Hoffmann, M. R. Patel, D. B. Mark, H. R. Al-Khalidi, B. Cavanaugh, J. Cole, R. J. Dolor, C. B. Fordyce, M. Huang, M. A. Khan, A. S. Kosinski, M. W. Krucoff, V. Malhotra, M. H. Picard, J. E. Udelson, E. J. Velazquez, E. Yow, L. S. Cooper, and K. L. Lee, "Outcomes of Anatomical versus Functional Testing for Coronary Artery Disease," N. Engl. J. Med. **372**(14), 1291–1300 (2015).
8. R. Heo, R. Nakazato, D. Kalra, and J. K. Min, "Noninvasive Imaging in Coronary Artery Disease," Semin. Nucl. Med. **44**(5), 398–409 (2014).
9. D. Engelbertsen, D. V. Anand, G. N. Fredrikson, D. Hopkins, R. Corder, P. K. Shah, A. Lahiri, J. Nilsson, and E. Bengtsson, "High levels of IgM against methylglyoxal-modified apolipoprotein B100 are associated with less coronary artery calcification in patients with type 2 diabetes," J. Intern. Med. **271**(1), 82–89 (2012).

Biomedical Optics EXPRESS

10. P. E. Morgan, P. J. Sheahan, D. I. Pattison, and M. J. Davies, "Methylglyoxal adversely affects the cellular redox balance in human coronary artery endothelial cells: A potential mechanism of action via modification of critical arginine residues," Free Radical Biol. Med. **53**, S147–S148 (2012).
11. M. G. A. van Eupen, M. T. Schram, H. M. Colhoun, J. L. J. M. Scheijen, C. D. A. Stehouwer, and C. G. Schalkwijk, "Plasma levels of advanced glycation endproducts are associated with type 1 diabetes and coronary artery calcification," Cardiovasc. Diabetol. **12**(1), 149 (2013).
12. V. Lankin, G. Konovalova, A. Tikhaze, K. Shumaev, E. Kumskova, and M. Viigimaa, "The initiation of free radical peroxidation of low-density lipoproteins by glucose and its metabolite methylglyoxal: a common molecular mechanism of vascular wall injure in atherosclerosis and diabetes," Mol. Cell. Biochem. **395**(1-2), 241–252 (2014).
13. M. Heier, H. D. Margeirsdottir, P. A. Torjesen, I. Seljeflot, K. H. Stensæth, M. Gaarder, C. Brunborg, K. F. Hanssen, and K. Dahl-Jørgensen, "The advanced glycation end product methylglyoxal-derived hydroimidazolone-1 and early signs of atherosclerosis in childhood diabetes," Diabetes Vasc. Dis. Res. **12**(2), 139–145 (2015).
14. Y. Dai, Y. Shen, Q. R. Li, F. H. Ding, X. Q. Wang, H. J. Liu, X. X. Yan, L. J. Wang, K. Yang, H. B. Wang, Q. J. Chen, W. F. Shen, R. Y. Zhang, and L. Lu, "Glycated Apolipoprotein A-IV Induces Atherogenesis in Patients With CAD in Type 2 Diabetes," J. Am. Coll. Cardiol. **70**(16), 2006–2019 (2017).
15. A. Moraru, J. Wiederstein, D. Pfaff, T. Fleming, A. K. Miller, P. Nawroth, and A. A. Teleman, "Elevated Levels of the Reactive Metabolite Methylglyoxal Recapitulate Progression of Type 2 Diabetes," Cell Metab. **27**(4), 926–934.e8 (2018).
16. I. Nemet, L. Varga-Defterdarović, and Z. Turk, "Preparation and quantification of methylglyoxal in human plasma using reverse-phase high-performance liquid chromatography," Clin. Biochem. **37**(10), 875–881 (2004).
17. M. Y. Khuhawar, A. J. Kandhro, and F. D. Khand, "Liquid Chromatographic Determination of Glyoxal and Methylglyoxal from Serum of Diabetic Patients using Meso-Stilbenediamine as Derivatizing Reagent," Anal. Lett. **39**(10), 2205–2215 (2006).
18. N. R. Neng, C. A. A. Cordeiro, A. P. Freire, and J. M. F. Nogueira, "Determination of glyoxal and methylglyoxal in environmental and biological matrices by stir bar sorptive extraction with in-situ derivatization," J. Chromatogr. A **1169**(1-2), 47–52 (2007).
19. Y. Ogasawara, R. Tanaka, S. Koike, Y. Horiuchi, M. Miyashita, and M. Arai, "Determination of methylglyoxal in human blood plasma using fluorescence high performance liquid chromatography after derivatization with 1,2-diamino-4,5-methylenedioxybenzene," J. Chromatogr. B: Anal. Technol. Biomed. Life Sci. **1029-1030**, 102–105 (2016).
20. K. Dhananjayan, F. Irrgang, R. Raju, D. G. Harman, C. Moran, V. Srikanth, and G. Münch, "Determination of glyoxal and methylglyoxal in serum by UHPLC coupled with fluorescence detection," Anal. Biochem. **573**, 51–66 (2019).
21. L. J. M. Scheijen Jean and G. Schalkwijk Casper, "Quantification of glyoxal, methylglyoxal and 3-deoxyglucosone in blood and plasma by ultra performance liquid chromatography tandem mass spectrometry: evaluation of blood specimen," Clin. Chem. Lab. Med. **52**(1), 85–91 (2014).
22. M. Pastor-Belda, A. J. Fernández-García, N. Campillo, M. D. Pérez-Cárceles, M. Motas, M. Hernández-Córdoba, and P. Viñas, "Glyoxal and methylglyoxal as urinary markers of diabetes. Determination using a dispersive liquid–liquid microextraction procedure combined with gas chromatography–mass spectrometry," J. Chromatogr. A **1509**, 43–49 (2017).
23. M. H. El-Maghrabey, T. Nakatani, N. Kishikawa, and N. Kuroda, "Aromatic aldehydes as selective fluorogenic derivatizing agents for α-dicarbonyl compounds. Application to HPLC analysis of some advanced glycation end products and oxidative stress biomarkers in human serum," J. Pharm. Biomed. Anal. **158**, 38–46 (2018).
24. N. Rabbani and P. J. Thornalley, "Measurement of methylglyoxal by stable isotopic dilution analysis LC-MS/MS with corroborative prediction in physiological samples," Nat. Protoc. **9**(8), 1969–1979 (2014).
25. C. Polson, P. Sarkar, B. Incledon, V. Raguvaran, and R. Grant, "Optimization of protein precipitation based upon effectiveness of protein removal and ionization effect in liquid chromatography–tandem mass spectrometry," J. Chromatogr. B: Anal. Technol. Biomed. Life Sci. **785**(2), 263–275 (2003).
26. J. Zhang, H. Zhang, M. Li, D. Zhang, Q. Chu, and J. Ye, "A novel capillary electrophoretic method for determining methylglyoxal and glyoxal in urine and water samples," J. Chromatogr. A **1217**(31), 5124–5129 (2010).
27. A. Shrivastava and V. Gupta, "Methods for the determination of limit of detection and limit of quantitation of the analytical methods," Chron. Young Sci. **2**(1), 21–25 (2011).